Westberry Toby, K. (Orcid ID: 0000-0003-3341-6080)
Shi Yingxi (Orcid ID: 0000-0001-5488-0777)
Behrenfeld Michael J. (Orcid ID: 0000-0003-1330-7098)

Satellite-detected Ocean Ecosystem Response to Volcanic Eruptions in the Subarctic Northeast Pacific Ocean

T.K. Westberry[1], Y. R. Shi[2,3], H. Yu[2], M.J. Behrenfeld[1] and L. A. Remer[3]

[1]Department of Botany and Plant Pathology, Oregon State University, Corvallis, OR, USA.

[2]Earth Science Division, NASA Goddard Space Flight Center, Greenbelt, MD, USA.

[3]Joint Center for Earth Systems Technology, University of Maryland – Baltimore County, Baltimore, MD, USA.

Corresponding author: Toby K. Westberry (toby.westberry@oregonstate.edu)

Key Points:

- The ash deposition from Aleutian volcanic eruptions in 2008 provides a case study for remote sensing analyses of ocean ecosystem response
- Clear signals are seen in bulk satellite properties and phytoplankton physiological indices (Chl:C and chlorophyll fluorescence yield)
- Ocean ecosystem response to iron fertilization is complex and can only be characterized with multiple satellite remote sensing products

This article has been accepted for publication and undergone full peer review but has not been through the copyediting, typesetting, pagination and proofreading process which may lead to differences between this version and the Version of Record. Please cite this article as doi: 10.1029/2019GL083977

Abstract

Volcanic eruptions in the Aleutian archipelago during the summer of 2008 deposited large quantities of iron-laden ash to the Subarctic North Pacific Ocean. The surface ocean ecosystem response has been previously characterized using limited in situ and autonomous field measurements and numerical modeling, but basin-scale satellite remote sensing has been limited to a simple description of chlorophyll variability. Here, we show that the ecosystem response is a complex combination of phytoplankton biomass and physiology that can be described with satellite ocean color diagnostics such as the chlorophyll to carbon biomass ratio ($Chl:C_{phyto}$) and chlorophyll fluorescence yield. Together, these quantities outline a more complete picture of ecological responses spanning unique signals of iron stress (and relief from), photoacclimation, changes in phytoplankton growth rate, increases in biomass, and timescales of decay for these processes.

Plain Language Summary

Phytoplankton growth in nearly one third of the global ocean is limited by the micronutrient iron. Outside the influence of continental margins, the only mechanisms to introduce new iron to the surface ocean is mixing up from the deep ocean (such as during winter storms) and through airborne deposition of desert dust. However, every once in a while large volcanic eruptions can provide a temporary source of iron to the ocean through deposition of volcanic ash. The effects of this "fertilization" are nearly impossible to measure in the field because of the unpredictability of volcanic eruptions. Satellite platforms provide the necessary coverage for this scale of event, but have been woefully underutilized to date. We revisit a pair of well documented volcanic eruptions from the Aleutian Archipelago and describe their impact on the surface ocean ecosystem of the Subarctic North Pacific Ocean using novel satellite-derived products supplemented by model output. We are able to characterize the ecosystem response in terms of both increased phytoplankton growth and adjustments in their physiology. The latter is often neglected, yet can be of equal or greater magnitude than changes in growth rate.

1 Introduction

The average global emission of volcanic ash (<63μm diameter) to the atmosphere is estimated at ~200 million tons yr^{-1} [Durant et al., 2010]. Some of this ash is deposited on the ocean's surface and the soluble nutrients it carries can be a significant contribution to phytoplankton nutrition [Achterberg et al., 2013; Langmann et al., 2010b; Olgun et al., 2011]. In the summer of 2008, the Okmok and Kasatoschi volcanoes on the Aleutian Archipelago underwent several eruptions in a relatively short period of time, resulting in large-scale delivery of ash-borne iron to the Eastern Subarctic Pacific Ocean. These "fertilization" events have been previously quantified using autonomous measurements, nearby field observations, and numerical modeling [Hamme et al., 2010; Lindenthal et al., 2013]. However, basin-scale characterization of marine ecosystem responses from satellite have been limited to a single property: chlorophyll concentration (Chl). Chlorophyll concentration by itself integrates information on phytoplankton abundance, nutrient and light physiological effects, and loss processes. Disentangling these processes is essential for properly interpreting the ecological and biogeochemical consequences of atmospheric iron deposition [Behrenfeld et al., 2015; Siegel et al., 2013b].

Recent advances in satellite remote sensing combined with a broad knowledge base on iron-mediated phytoplankton physiology (see review by Behrenfeld and Milligan [2013]) allow for a far more complete description of ecosystem responses following large-scale iron enrichment [Westberry et al., 2013]. The Okmok and Kasatoschi eruptions in 2008 provide a perfect opportunity to demonstrate this capability due to their well-defined eruption timelines [Waythomas et al., 2010] and their proximity to a permanently iron-impoverished ocean region (the Eastern Subarctic Pacific Ocean).

1.1 Iron-stress phytoplankton physiology

Regional iron limitation of phytoplankton productivity was first proposed by Haaken Gran in 1932 [Gran, 1932], but it wasn't until the latter decades of the 20th century that this idea was experimentally confirmed in natural phytoplankton populations [Martin & Fitzwater, 1988; Martin et al., 1991]. Detailed insights on the physiological consequences of iron stress have since emerged from targeted laboratory studies [Greene et al., 1992; Sunda & Huntsman, 1997], field measurements [Kolber et al., 1994; Price et al., 1991], and natural [Blain et al., 2008; Blain et al., 2001] and purposeful mesoscale iron enrichments (see reviews by de Baar et al. [2005] and Boyd et al. [2007]). Two specific physiological consequences of iron fertilization of relevance to remote sensing are changes in phytoplankton pigment concentrations per unit biomass and changes in chlorophyll fluorescence yields.

To optimize light or nutrient limited growth rates, phytoplankton highly regulate their light harvesting capacity (i.e., pigment concentration) to match metabolic demands for photosynthesis [Halsey & Jones, 2015; Laws & Bannister, 1980]. Under nutrient-replete conditions, the amount of chlorophyll per unit cellular carbon (Chl:C, mg mg^{-1} hereafter

dimensionless) varies linearly with phytoplankton growth rate (μ) and is determined by the acclimation (or growth) irradiance. Changes in Chl:C in this context are termed "photoacclimation" [Falkowski & Laroche, 1991] and can be fairly well-modeled from satellite retrieved properties [Behrenfeld et al., 2015]. Thus, observed changes in Chl:C can be partitioned between those due to growth rate or photoacclimation (for changes associated with phytoplankton community composition, see discussion in Section 3.2.2).

Iron stress causes unique physiological features in phytoplankton because iron is an abundant cofactor in photosynthetic and metabolic machinery [Sunda & Huntsman, 1995; Sunda & Huntsman, 1997]. Although a diversity of physiological responses to iron stress can be found across phytoplankton taxa [Marchetti and Harrison, 2007; Strzepek et al., 2019], there are many conserved characteristics behaviors. In particular, phytoplankton grown under iron-limiting conditions and in the presence of sufficient macronutrients (a condition in the ocean referred to as high-nutrient, low-chlorophyll (HNLC)) retain excess Chl beyond that required to maintain their iron-determined growth rate [Behrenfeld & Milligan, 2013; Behrenfeld et al., 2006; Schrader et al., 2011]. This excess chlorophyll is bound to proteins in structures that are not photosynthetically active, but are mobilized upon release from iron stress. One important consequence of these structures is that they cause iron-limited phytoplankton populations to exhibit enhanced fluorescence emission. This effect has allowed fluorescence yields to be used to diagnose iron stress in the field, to spatially map iron limited phytoplankton populations, and to detect initial physiological response to iron enrichment [Behrenfeld et al., 2006; Boyd & Abraham, 2001; Boyd et al., 2005; Kolber et al., 1994]. Importantly, phytoplankton Chl:C and chlorophyll fluorescence are two properties that can now be monitored from space.

1.2 Remote sensing of physiology and iron deposition responses

The ability to independently retrieve pigment (Chl) and biomass (C_{phyto}) from satellite ocean color data has opened the door to assessing phytoplankton physiology from space [Behrenfeld et al., 2005; Siegel et al., 2013a]. As noted above, Chl:C contains information about photoacclimation and nutrient stress and has been exploited to improve models of net primary production and growth [Westberry et al., 2008]. Analyses of satellite Chl:C data has also demonstrated that the majority of Chl variability observed throughout the permanently stratified ocean (~45°S-45°N) is due to physiological adjustments in cellular pigmentation [Behrenfeld et al., 2005; Siegel et al., 2013a], and that the light-driven component of Chl:C can be well-modeled with information about the mixed-layer light environment [Behrenfeld et al., 2015]. The remaining Chl:C variability is due to nutrient stress and associated changes in growth rate, which in HNLC regions are due to iron deficiency.

Satellite fluorescence data have also been used to detect iron-stressed phytoplankton populations and responses to iron enrichment at the global [Behrenfeld et al., 2009], regional [Westberry et al., 2016], and event [Westberry et al., 2013] scales. These studies have documented elevated fluorescence yields in chronically iron-limited regions (e.g., the Equatorial Pacific) and decreased fluorescence yields following natural or purposeful iron

addition in these regions. Mechanisms behind these responses are discussed further in Section 3.2.3.

The current study uses diverse atmospheric and ocean satellite remote sensing products supplemented by model output to gain greater insight into the surface ocean ecosystem response to Okmok and Kasatoschi ash deposition of iron. Specifically, we examine time series of bulk biological properties (Chl and C_{phyto}), and growth/physiological indicators (Chl:C and chlorophyll fluorescence) estimated from ocean color satellite data across the transition from iron-limited to non-limiting conditions. Patterns in each property are interpreted in the context of known phytoplankton physiology.

2 Data and Methods

2.1 Satellite products

Atmospheric remote sensing products were used to characterize the extent and timeline of volcanic ash introduced to the atmosphere and surface ocean. MODIS-Terra brightness temperature difference between 11 and 12 μm wavelength ($\Delta BT_{11\text{-}12}$) in clear sky conditions was used as the primary ash detection diagnostic [Langmann et al., 2010a; Pavolonis et al., 2006; Pavolonis et al., 2013; Prata, 1989]. The $\Delta BT_{11\text{-}12}$ was calculated from Level 1B data (MOD021KM and MYD21KM) acquired from the NASA Level 1 and Atmospheric Archive & Distribution System Data Active Archive Center (LAADS DAAC, https://ladsweb.modaps.eosdis.nasa.gov). Daily $\Delta BT_{11\text{-}12}$ were aggregated into 4-day composites. Visual validation of ash plumes also made use of daytime MODIS true-color composite imagery contained in the NASA Worldview catalog (https://worldview.earthdata.nasa.gov).

Standard operational satellite ocean color products were obtained from the NASA Ocean Biology Data Active Archive Center (OB.DAAC, https://oceancolor.gsfc.nasa.gov). Daily and monthly Level 3 MODIS-Aqua products (~9km spatial resolution) were used in this analysis and consisted of chlorophyll concentration (Chl, mg m^{-3}), diffuse attenuation at 490 nm (Kd490, m^{-1}), particulate backscattering at 443 nm (bbp, m^{-1}), daily incident broadband irradiance (PAR, Ein m^{-2} d^{-1}), instantaneous broadband irradiance (iPAR, mEin m^{-2} s^{-1}), and normalized fluorescence line height (nFLH, W m^{-2} μm^{-1} sr^{-1}). nFLH quantifies the fluorescence contribution to water-leaving radiance and contains information about pigment biomass and phytoplankton physiology [Huot et al., 2005; Behrenfeld et al., 2009]. Particulate backscattering was estimated using the Generalized Inherent Optical Property (GIOP) model [Werdell et al., 2013] and converted to phytoplankton carbon biomass [Behrenfeld et al., 2005; Graff et al., 2015; Westberry et al., 2008]. Daily products were used to create 4-day composites, while monthly products were used to construct mission-era climatologies (2003-2017).

2.2 Model data

To supplement the MODIS-based ash plume tracking with $\Delta BT_{11\text{-}12}$, we use aerosol deposition flux from the Modern-Era Retrospective analysis for Research and Applications Version 2 (MERRA2) to illustrate spatio-temporal patterns in ash deposition. The MERRA2

is a global atmospheric data assimilation reanalysis that spans the modern satellite observing era (1980-present) [Gelaro et al., 2017]. It is important to note that the distribution of airborne particles reflected in aerosol optical depth (AOD) or $\Delta BT_{11\text{-}12}$ is not always correlated with the aerosol deposition onto the sea surface. In the MERRA2 reanalysis, the MODIS measured clear-sky radiance is used to constrain the aerosol loading in the atmosphere [Randles et al., 2017]. This aerosol assimilation technique enhances the model's capability of capturing unexpected episodic events such as volcanic eruptions for which ash emissions are hard to quantify. While aerosol loading is constrained by observations, deposition is not and therefore quantification of deposition is subject to additional uncertainty associated with model representation of aerosol removal (e.g., dry deposition and cloud/precipitation scavenging). In this study, we use the aerosol deposition fluxes to identify the locations of ash deposition, but not to accurately quantify the amount.

To fully understand the physiological basis of satellite-observed changes in phytoplankton Chl:C in response to the Okmok and Kasatoschi eruptions, a quantification of light-driven photoacclimation is required. This photoacclimation response is a function of the mixed layer light level, which is defined by PAR, Kd490, and mixed layer depth (MLD). The MLD is not a property directly retrieved from satellites but is provided by Hybrid Coordinate Model (HYCOM) hindcast simulations [Chassignet et al., 2007]. For the current study, MLD was defined by a density threshold criteria of 0.03 kg m^{-3} [de Boyer Montegut et al., 2004; Holte & Talley, 2009]. Similar to the ocean color products, MLD was calculated on a daily basis and averaged into 4-day composites.

3 Results

3.1 Characterization of volcanic ash plumes and deposition

Ash plumes from the Okmok and Kasatoschi eruptions are clearly evident in our remote sensing and model-based products. When averaged over a broad region (44-54°N, 135-175°W), the ash brightness temperature product ($\Delta BT_{11\text{-}12}$) decreases following the initial Okmok eruption (Jul 21, YD 201) and then decreases more significantly following the Kasatoschi eruption (Aug 7-9, YD 220-222) (Figure 1a). If the averaging region is constrained to a much smaller area nearer to the volcanoes, the $\Delta BT_{11\text{-}12}$ decrease after the Okmok eruption becomes more pronounced than observed in the broader areal average (see Larsen et al. [2009]). The 4-day composite $\Delta BT_{11\text{-}12}$ encompassing the Kasatoschi eruption illustrates the spatial extent and transport of the ash signal across much of the eastern subarctic Pacific (Figure 1b). Approximately 5.7×10^6 km^2 of the study region exhibited decreased $\Delta BT_{11\text{-}12}$ during this post-eruption 4-day period, as compared to a 4-day period one week prior to either eruption (YD 194-197). Langmann et al. [2010a] estimated that >90% of the ash emitted by Kasatoschi was deposited into the eastern subarctic Pacific prior to reaching the North American continent.

MERRA2-based aerosol deposition indicates that ash deposition from the Okmok eruption was much smaller in spatial extent than Kasatoschi (Figure 1c). Ash deposition from Okmok, however, is much larger over a more restricted region closer to the volcanic site (not shown). The 4-day period following the Kasatoschi eruption shows widespread

deposition throughout the subarctic Pacific (Figure 1d). Previous model-based estimates explicitly including the Kasatoschi eruption estimate a deposition of ~10^{12} kg ash to the surface ocean following the event [Langmann et al., 2010a; Langmann et al., 2010b].

3.2 Ocean ecosystem responses

3.2.1 Bulk properties

Extended time-series of phytoplankton Chl and carbon biomass concentration (C_{phyto}) for 2008 (including the two eruption periods) are shown in Figure 2a & 2b. Chlorophyll shows distinct responses to both the Okmok eruption and to the larger Kasatoschi eruption (Figure 2a). These increases in chlorophyll were sustained for ~2 months following the eruptions. This prolonged response is consistent with observations from the Southern Ocean where iron-mediated ecosystem changes following enrichment persisted for months, apparently due to efficient recycling of iron through the grazer community [Bowie et al., 2001; Boyd et al., 2000]. For our subarctic Pacific analysis, we find that the Okmok Chl feature is short-lived (<14 days) and yet significant, with values increasing by ~140% (from 0.2 to 0.5 mg m^{-3}). The larger Chl signal following Kasatoschi (Fig. 2a) has been noted as the single largest feature in the entire modern satellite record for the eastern Subarctic Pacific [Hamme et al., 2010], with widespread peak Chl values of >1 mg m^{-3} (i.e., 37% of valid pixels had peak Chl values exceeding 1 mg m^{-3}). Spatial variability (indicated by the error bars during each 4 day composite value in Figure 2a) was also much higher following the Okmok and Kasatoschi eruptions than during the preceding months.

Interestingly, the C_{phyto} record shows both similarities and differences from Chl across the two volcanic events (Figure 2b). An obvious major difference is the Okmok eruption elicited only a minimal change in C_{phyto} (p=0.06, two-tailed T-test between one week prior to and after eruption). This difference suggests that much of the Chl response reflected physiological (rather than biomass) impacts of the iron deposition (see next section). In contrast, the Kasatoschi eruption yielded a large increase in C_{phyto} over the first ~2 weeks that paralleled changes in Chl, with C_{phyto} values more than doubling from ~30 to 70 mg m^{-3}. This increase occurred during the typical annual peak in C_{phyto} [Westberry et al., 2016], which itself is more than a doubling of biomass over winter concentrations. The elevated biomass response to Kasatoschi persisted into October, similar to the Chl record. It is unlikely that these findings reflect changes in satellite ocean color retrieval coverage because there is no significant difference in viewable area before nor after each eruption or any significant difference from mission-era climatological coverage (Figure 2c).

3.2.2 Physiology and the Chl:C ratio

Differential responses in the post-eruption Chl and C_{phyto} time series (Figure 2a&b) register the temporal physiological regulation of cellular Chl:C. Quantitatively, Chl:C changes in the region influenced by volcanic ash deposition show a >3-fold increase from pre-eruption conditions (0.005) to maximum values in mid-August (0.016) (Figure 3a). An initial Chl:C increase is observed following the Okmok eruption that subsides briefly before

being followed by an additional increase in response to the Kasatoschi eruption. These observed increases in Chl:C can be segregated into a component due to photoacclimation and a component reflecting growth rate changes from ash-derived iron addition.

Throughout the eruption period and spanning the boreal summer, surface ocean mixed layer depths were stable in the subarctic Pacific (20.2 ± 3.2 meters for Jul-Aug, YD 182-243) and consistent with climatological mean values (Figure 3b). Thus, any photoacclimation contribution to Chl:C changes will reflect changes in the mixed layer light environment due to changes in incident light (PAR) and diffuse attenuation (K_d). The more significant of these two factors was an increase in K_d following each eruption due to consequential increases in chlorophyll and a reduction in the euphotic depth (dotted line in Figure 3b). Applying the photoacclimation model of Behrenfeld et al. [2015] to our satellite ocean color and mixed layer depth data over this time period, indicates that approximately half of the observed Chl:C increase was due to photoacclimation (red curve in Figure 3a). What this means is that the remaining Chl:C changes are reflective of iron-induced changes (increases) in growth rate. Since the Chl:C increase following Okmok was not accompanied by any significant increase in phytoplankton biomass, the changes in growth rate must have been matched by concurrent losses (e.g., increased grazing). This suggestion is consistent with Kasatoschi ash-incubation results showing a threshold in net primary production rates (and growth) required before biomass increases were observed (see Figures 2 and 4 in Melancon et al. [2014]). The extent of Chl:C response can be seen throughout the region as sustained positive anomalies in Chl:C (ΔChl:C, red areas in Figure 3c). The median ΔChl:C (relative to seasonal averages) is +51%, while anomalies >100% are widespread and occur in 20% of the pixels (Figure 3d).

Chl:C differences may also arise from changes in phytoplankton community composition [Cetinic et al., 2015]. This can be due to changes in the ratio of accessory pigments to Chl [Macintyre et al., 2002] or due to changes in cell size [Six et al., 2008; Fujiki and Taguchi, 2002]. In either case, these changes would occur in the opposite direction as changes in Chl:C due to photoacclimation and growth rate. That is, while we observe substantial increases in Chl:C across the transition of iron fertilization, taxonomic changes in Chl:C would act to mitigate this pattern (i.e., decrease from higher to lower Chl:C). There is likely a component of ΔChl:C due to changes in species composition, but it is currently difficult to diagnose from satellite ocean color data [Brewin et al., 2011; Hirata et al., 2012].

The current findings, once again, point to the significant role that physiology plays in chlorophyll variability. Early recognition of seasonal Chl:C variability in the Subarctic Pacific Ocean documented a >3-fold change between winter and summer due to photoacclimation [McAllister, 1969]. These findings were formalized in subsequent regional modeling studies [Frost, 1987]. Further evidence from laboratory, field, and in situ studies in the eastern subarctic Pacific consistently show Chl:C increases of approximately 2-6 times upon addition of iron [Boyd et al., 2005; Coale, 1991; Marchetti & Harrison, 2007; Sunda & Huntsman, 1995]. For example, during the Subarctic Ecosystem Response to Iron Enrichment Study (SERIES) in this region, measured values of Chl:C increased from 0.0083

to 0.025 (i.e., C:Chl decreased from 120 to 40 g:g) in the iron-stimulated bloom [Boyd et al., 2005]. Bishop et al. [2002] inferred similar Chl:C changes in response to natural dust iron deposition in the region by combining satellite estimates of Chl and profiling-float based estimates of particulate carbon. Clearly, the assumption of a fixed Chl:C across the Okmok and Kasatoschi eruption response would result in significant biases in phytoplankton biomass or subsequent calculations (e.g., CO_2 uptake, export production, elemental budgets).

3.2.3 Chlorophyll fluorescence

Further insight into the physiological response of phytoplankton to the Okmok and Kasatoschi eruptions can be gained from the satellite fluorescence record. In order to isolate the iron-specific fluorescence response, nFLH must first be normalized to pigment concentration and incident light (to account for non-photochemical quenching, NPQ) and expressed as the NPQ-corrected fluorescence yield, $(nFLH/Chl)_{corr}$. Although the fluorescence time-series is generally noisier than other ocean color products, sharp decreases in $(nFLH/Chl)_{corr}$ are clearly seen following both eruption events (Figure 4a). These decreases are consistent with expectations for relief from iron stress [Westberry et al., 2013] and are characterized by a rapid decrease in fluorescence yields to local minima immediately following deposition. We further find that $(nFLH/Chl)_{corr}$ returns to pre-eruption values within ~2 weeks following the Okmok event, whereas the sharp decrease following Kasatoschi iron deposition is followed by sustained low values (which remain below climatological values) for the duration of elevated Chl and biomass (i.e., nearly two months until October). Bowie et al. [2001] inferred that biological iron cycling (via regeneration by grazers) was self-sustaining in the Southern Ocean Iron Release Experiment (SOIREE), allowing the resultant bloom to continue growing >40 days after iron fertilization. A similar scenario may have unfolded in the subarctic Pacific following Kasatoschi ash deposition, postponing the re-establishment of iron limitation and keeping the fluorescence signal depressed. The monthly composite fluorescence yield anomaly $\Delta(nFLH/Chl)_{corr}$ over the region during August clearly shows a widespread, coherent pattern of decreased fluorescence yield (blue areas in Figure 4b). Approximately 1.6 million km^2 (49%) of the study region exhibited negative $\Delta(nFLH/Chl)_{corr}$ during the month of August. $\Delta(nFLH/Chl)_{corr}$ in this feature are 30-50% less than climatological averages (Figure 4c).

Enhanced fluorescence under iron-stress reflects, in part, the dysfunctional pigment protein complexes described previously and also a stoichiometric change in photosynthetic membranes. More specifically, iron-stressed phytoplankton populations tend to have a higher concentration of the oxygen-evolving photosynthetic reaction centers (PSII) relative to the non-oxygen-evolving and high iron-demanding centers (PSI) (but see Strzepek et al. [2019]). As PSII is the dominant source of chlorophyll fluorescence, an increase in PSII:PSI in iron-stressed populations means that fluorescence per unit chlorophyll (i.e., fluorescence yield)

will be higher [Behrenfeld & Milligan, 2013; Berges et al., 1996; Greene et al., 1991; Ivanov et al., 2000; Krause & Weis, 1991; Strzepek & Harrison, 2004].

3.3 Discussion and next steps

One finding from this analysis that is particularly interesting is the timescale of ecosystem response following deposition. In a typical (non-HNLC) temperate ocean region with recurrent seasonal cycles in phytoplankton biomass, the time-averaged rates of accumulation are small due to incremental increases in growth conditions (nutrients and/or light availability). In other words, the biomass accumulation is driven by small accelerations in growth rate. For example, the phytoplankton population need only double ~4-6 times to increase from the mid-winter minimum to the summer maximum observed biomass, assuming no losses [Behrenfeld, 2014]. However, this relatively modest increase requires many months to achieve, and phytoplankton divide 10-100 times the required number of doublings in the same time period, highlighting the tight coupling between growth and loss. In contrast, the massive volcanic deposition from Kasatoschi allowed for a rapid accumulation of biomass in only 1-2 weeks. This is possible because it provides a large acceleration in growth rate as the phytoplankton quickly transition from severe iron-limitation to non-limiting conditions.

Peak Chl and C_{phyto} was reached 9-12 days after the Kasatoschi eruption (YD 229-232, mid-August), similar to purposeful mesoscale iron enrichment experiments in the subarctic North Pacific [Boyd et al., 2004; Tsuda et al., 2003] and elsewhere [Behrenfeld & Boss, 2014]. However, the decline following the natural fertilization is significantly slower than found in most mesoscale iron enrichment experiments. In the Subarctic Ecosystem Response to Iron Enrichment Study (SERIES) in this same region, the bloom decline began ~17-18 days after fertilization and most ecological indicators (including Chl) returned to near-climatological levels within 10 days thereafter. Thus, the ecosystem quickly returned to near-normal within ~25 days. The decline phase of the Kasatoschi bloom extended for nearly 50 days, despite the bloom peak being much smaller than observed during SERIES (Chl ~ 1.0 mg m^{-3} versus 5.0 mg m^{-3}). The potential reasons for this difference are difficult to diagnose from a remote sensing perspective, but are likely related to the large spatial scale of the fertilization compared with purposeful mesoscale enrichments and the significance of dilution through the patch edges (e.g., Abraham et al. [2000]). The magnitude of the bloom compared with many mesoscale iron-enrichment experiments may also have facilitated less aggregation and altered sinking from the euphotic zone (e.g., Waite and Nodder [2001]). Other factors could be related to differences in available nutrients (e.g., Boyd et al. [2005]) and responses of the grazer community.

Our ability to observe and monitor ecosystem response to episodic forcing has never been better. The consistent story presented here is encouraging and suggests that distinguishing ecosystem response to deposition from the background of natural variability is possible despite a number of challenges from the satellite perspective (e.g., cloud coverage and sampling bias from co-occurrence with wet deposition events). For example, the values shown in the time series of Chl and C_{phyto} clearly demonstrate a strong ecosystem response to

ash deposition despite representing approximately 20% of the study region at any given time (Figure 2c). However, the observed patterns of ocean color properties and their interpretation here were made possible largely because the time and location to investigate were known a priori and there was an understanding of expected physiological stresses. This demonstration is a critical step towards examining the full global ocean color record for responses to large scale iron addition via volcanic or dust deposition, but clearly more information will be needed. Knowledge of the frequency and extent of deposition events will be key, as will defining regions of ecosystem response. To this end, it is preferable to use observable satellite properties to dynamically define regions of response, rather than arbitrarily outlining geographic bins. This distinction may be particularly important in ocean regions that undergo transient iron limitation during some parts of the year.

4 Conclusions

We present here a case study of ocean ecosystem response to an airborne fertilization event, which took place over a region of approximately 6 million km^2 and lasted nearly three months. The full extent of this event could only be captured by the spatial and temporal coverage of satellite observations, but past studies of large scale, in situ iron fertilization have been limited to simple descriptions of chlorophyll variability. Our analysis shows the need for multiple satellite indices to fully describe the chain of events affecting the physiological and ecosystem response, and that chlorophyll alone is inadequate. Differentiating biomass from physiological response in the phytoplankton is critical for interpreting biogeochemical consequences. Furthermore, consideration of interactions between trophic levels reveals that small signals in some observable properties (e.g., biomass) may underlie larger biogeochemical responses. The techniques and approach used here provide a path toward broader analyses for evaluating the significance of global aeolian deposition on surface ocean ecosystem processes. Quantitatively establishing this atmosphere-ocean link will be particularly important as we consider long-term secular changes in these systems.

Acknowledgments

All atmospheric and ocean satellite data products are freely available through their respective NASA data centers (LAADS DAAC and OB.DAAC). Funding for this work was provided by NASA to L.A.R. (Grant #80NSSC18K0953) and T.K.W. (Grant #80NSSC18K0616).

References

Abraham, E., Law, C.S., Boyd, P.W., Lavender, S.J., Maldonado, M.T., Bowie, A.R. (2000), Importance of stirring in the development of an iron-fertilized phytoplankton bloom. Nature 407, 727}730.

Achterberg, E. P., Moore, C. M., Henson, S. A., Steigenberger, S., Stohl, A., Eckhardt, S., et al. (2013), Natural Iron Fertilization by the Eyjafjallajokull Volcanic Eruption, *Geophysical Research Letters*, *40*(5), 921-926.

Behrenfeld, M. J. (2014), Climate-Mediated Dance of the Plankton, *Nature Climate Change*, *4*(10), 880-887.

Behrenfeld, M. J., & Boss, E. S. (2014), Resurrecting the Ecological Underpinnings of Ocean Plankton Blooms, *Annual Review of Marine Science, Vol 6*, *6*, 167-U208.

Behrenfeld, M. J., & Milligan, A. J. (2013), Photophysiological Expressions of Iron Stress in Phytoplankton, in *Annual Review of Marine Science, Vol 5*, edited by C. A. Carlson and S. J. Giovannoni, pp. 217-246.

Behrenfeld, M. J., Boss, E., Siegel, D. A., & Shea, D. M. (2005), Carbon-Based Ocean Productivity and Phytoplankton Physiology from Space, *Global Biogeochemical Cycles*, *19*(1), 1-14, doi:10.1029/2004GB002299.

Behrenfeld, M. J., Worthington, K., Sherrell, R. M., Chavez, F. P., Strutton, P., McPhaden, M., & Shea, D. M. (2006), Controls on Tropical Pacific Ocean Productivity Revealed through Nutrient Stress Diagnostics, *Nature*, *442*(7106), 1025-1028.

Behrenfeld, M. J., O'Malley, R. T., Boss, E., Westberry, T. K., Graff, J. R., Halsey, K. H., et al. (2015), Revaluating Ocean Warming Impacts on Global Phytoplankton, *Nature Climate Change*.

Behrenfeld, M. J., Westberry, T. K., Boss, E. S., O'Malley, R. T., Siegel, D. A., Wiggert, J. D., et al. (2009), Satellite-Detected Fluorescence Reveals Global Physiology of Ocean Phytoplankton, *Biogeosciences*, *6*, 779-794.

Berges, J. A., Charlebois, D. O., Mauzerall, D. C., & Falkowski, P. G. (1996), Differential Effects of Nitrogen Limitation on Photosynthetic Efficiency of Photosystems I and Ii in Microalgae, *Plant Physiology*, *110*(2), 689-696.

Bishop, J. K. B., Davis, R. E., & Sherman, J. T. (2002), Robotic Observations of Dust Storm Enhancement of Carbon Biomass in the North Pacific, *Science*, *298*(5594), 817-821.

Blain, S., Sarthou, G., & Laan, P. (2008), Distribution of Dissolved Iron During the Natural Iron-Fertilization Experiment Keops (Kerguelen Plateau, Southern Ocean), *Deep-Sea Research Part II*, *55*(5-7), 594-605.

Blain, S., Treguer, P., Belviso, S., Bucciarelli, E., Denis, M., Desabre, S., et al. (2001), A Biogeochemical Study of the Island Mass Effect in the Context of the Iron Hypothesis: Kerguelen Islands, Southern Ocean, *Deep-Sea Research Part I*, *48*(1), 163-187.

Bowie, A. R., Maldonado, M. T., Frew, R. D., Croot, P. L., Achterberg, E. P., Mantoura, R. F. C., et al. (2001), The Fate of Added Iron During a Mesoscale Fertilisation Experiment in the Southern Ocean, *Deep-Sea Research Part Ii-Topical Studies in Oceanography*, *48*(11-12), 2703-2743.

Boyd, P. W., & Abraham, E. R. (2001), Iron-Mediated Changes in Phytoplankton Photosynthetic Competence During Soiree, *Deep-Sea Research Part II*, *48*(11-12), 2529-2550.

Boyd, P. W., Strzepek, R., Takeda, S., Jackson, G., Wong, C. S., McKay, R. M., et al. (2005), The Evolution and Termination of an Iron-Induced Mesoscale Bloom in the Northeast Subarctic Pacific, *Limnology and Oceanography*, *50*(6), 1872-1886.

Boyd, P. W., Jickells, T., Law, C. S., Blain, S., Boyle, E. A., Buesseler, K. O., et al. (2007), Mesoscale Iron Enrichment Experiments 1993-2005: Synthesis and Future Directions, *Science*, *315*(5812), 612-617.

Boyd, P. W., Watson, A. J., Law, C. S., Abraham, E. R., Trull, T., Murdoch, R., et al. (2000), A Mesoscale Phytoplankton Bloom in the Polar Southern Ocean Stimulated by Iron Fertilization, *Nature*, *407*(6805), 695-702.

Boyd, P. W., Law, C. S., Wong, C. S., Nojiri, Y., Tsuda, A., Levasseur, M., et al. (2004), The Decline and Fate of an Iron-Induced Subarctic Phytoplankton Bloom, *Nature*, *428*(6982), 549-553.

Brewin, R.J., Hardman-Mountford, N.J., Lavender, S.J., Raitsos, D.E., Hirata, T., Uitz, J., Devred, E., Bricaud, A., Ciotti, A., Gentili, B. (2011) An inter-comparison of bio-optical techniques for detecting dominant phytoplankton size class from satellite remote sensing. Remote Sens. Environ. 115 (2), 325–339.

Cetinić, I., M. J. Perry, E. D'Asaro, N. Briggs, N. Poulton, M. E. Sieracki, and C. M. Lee (2015), A simple optical index shows spatial and temporal heterogeneity in phytoplankton community composition during the 2008 North Atlantic Bloom Experiment, Biogeosciences, 12(7), 2179–2194, doi:10.5194/bg-12-2179-2015.

Chassignet, E. P., Hurlburt, H. E., Smedstad, O. M., Halliwell, G. R., Hogan, P. J., Wallcraft, A. J., et al. (2007), The Hycom (Hybrid Coordinate Ocean Model) Data Assimilative System, *Journal of Marine Systems*, *65*(1-4), 60-83.

Coale, K. H. (1991), Effects of Iron, Manganese, Copper, and Zinc Enrichments on Productivity and Biomass in the Sub-Arctic Pacific, *Limnology and Oceanography*, *36*(8), 1851-1864.

de Baar, H. J. W., Boyd, P. W., Coale, K. H., Landry, M. R., Tsuda, A., Assmy, P., et al. (2005), Synthesis of Iron Fertilization Experiments: From the Iron Age in the Age of Enlightenment, *Journal of Geophysical Research*, *110*(C9).

de Boyer Montegut, C., Madec, G., Fischer, A. S., Lazar, A., & Iudicone, D. (2004), Mixed Layer Depth over the Global Ocean: An Examination of Profile Data and a Profile-Based Climatology, *Journal of Geophysical Research-Oceans*, *109*(C12).

Durant, A. J., Bonadonna, C., & Horwell, C. J. (2010), Atmospheric and Environmental Impact of Volcanic Particulates, *Elements*, *6*(4), 235-240.

Falkowski, P. G., & Laroche, J. (1991), Acclimation to Spectral Irradiance in Algae, *Journal of Phycology*, *27*(1), 8-14.

Frost, B. W. (1987), Grazing Control of Phytoplankton Stock in the Open Sub-Arctic Pacific Ocean - a Model Assessing the Role of Mesozooplankton, Particularly the Large Calanoid Copepods *Neocalanus* Spp. , *Marine Ecology Progress Series*, *39*(1), 49-68.

Fujiki, T. and S. Taguchi (2002) Variability in chlorophyll a specific absorption coefficient in marine phytoplankton as a function of cell size and irradiance. J. Plankton Research 24(9): 859-874.

Gelaro, R., McCarty, W., Suarez, M. J., Todling, R., Molod, A., Takacs, L., et al. (2017), The Modern-Era Retrospective Analysis for Research and Applications, Version 2 (Merra-2), *Journal of Climate*, *30*(14), 5419-5454.

Graff, J. R., Westberry, T. K., Milligan, A. J., Brown, M. B., Dall'Olmo, G., van Dongen-Vogels, V., et al. (2015), Analytical Phytoplankton Carbon Measurements Spanning Diverse Ecosystems, *Deep-Sea Research I*, *102*, 16-25.

Gran, H. H. (1932), Phytoplankton. Methods and Problems, *Journal du Conseil Permanent Internationale pour L'Exploration de la Mer.*, *7*, 343-358.

Greene, R. M., Geider, R. J., & Falkowski, P. G. (1991), Effect of Iron Limitation on Photosynthesis in a Marine Diatom, *Limnology and Oceanography*, *36*(8), 1772--1782.

Greene, R. M., Geider, R. J., Kolber, Z., & Falkowski, P. G. (1992), Iron-Induced Changes in Light Harvesting and Photochemical Energy-Conversion Processes in Eukaryotic Marine-Algae, *Plant Physiology*, *100*(2), 565--575.

Halsey, K. H., & Jones, B. M. (2015), Phytoplankton Strategies for Photosynthetic Energy Allocation, *Annual Review of Marine Science, Vol 7*, *7*, 265-297.

Hamme, R. C., Webley, P. W., Crawford, W. R., Whitney, F. A., DeGrandpre, M. D., Emerson, S. R., et al. (2010), Volcanic Ash Fuels Anomalous Plankton Bloom in Subarctic Northeast Pacific, *Geophysical Research Letters*, *37*.

Hirata, T., Hardman-Mountford, N., Brewin, R.J.W. (2012), Comparing satellite-based phytoplankton classification methods. EOS Trans. Am. Geophys. Union 93 (6), 59.

Holte, J., & Talley, L. (2009), A New Algorithm for Finding Mixed Layer Depths with Applications to Argo Data and Subantarctic Mode Water Formation, *Journal of Atmospheric and Oceanic Technology*, *26*(9), 1920-1939.

Hu, C. M., Feng, L., Lee, Z., Davis, C. O., Mannino, A., McClain, C. R., & Franz, B. A. (2012), Dynamic Range and Sensitivity Requirements of Satellite Ocean Color Sensors: Learning from the Past, *Applied Optics*, *51*(25), 6045-6062.

Huot, Y., Brown, C. A. and Cullen, J. J.(2005), New algorithms for MODIS sun-induced chlorophyll fluorescence and a comparison with present data products, Limnol. Oceanogr. Methods, 3, 108–130.

Ivanov, A. G., Park, Y. I., Miskiewicz, E., Raven, J. A., Huner, N. P. A., & Oquist, G. (2000), Iron Stress Restricts Photosynthetic Intersystem Electron Transport in Synechococcus Sp, Pcc 7942, *Febs Letters*, *485*(2-3), 173-177.

Kolber, Z. S., Barber, R. T., Coale, K. H., Fitzwater, S. E., Greene, R. M., Johnson, K. S., et al. (1994), Iron Limitation of Phytoplankton Photosynthesis in the Equatorial Pacific-Ocean, *Nature*, *371*(6493), 145-149.

Krause, G. H., & Weis, E. (1991), Chlorophyll Fluorescence and Photosynthesis - the Basics, *Annual Review of Plant Physiology and Plant Molecular Biology*, *42*, 313-349.

Langmann, B., Zaksek, K., & Hort, M. (2010a), Atmospheric Distribution and Removal of Volcanic Ash after the Eruption of Kasatochi Volcano: A Regional Model Study, *Journal of Geophysical Research-Atmospheres*, *115*.

Langmann, B., Zaksek, K., Hort, M., & Duggen, S. (2010b), Volcanic Ash as Fertiliser for the Surface Ocean, *Atmospheric Chemistry and Physics*, *10*(8), 3891-3899.

Larsen, J., Neal, C., Webley, P., Freymueller, J., Haney, M., McNutt, S., et al. (2009), Eruption of Alaska Volcano Breaks Historic Pattern, *EoOS Transactions AGU*, *90*(20), 173-174.

Laws, E. A., & Bannister, T. T. (1980), Nutrient-Limited and Light-Limited Growth of Thalassiosira-Fluviatilis in Continuous Culture, with Implications for Phytoplankton Growth in the Ocean, *Limnology and Oceanography*, *25*(3), 457-473.

Lindenthal, A., Langmann, B., Paetsch, J., Lorkowski, I., & Hort, M. (2013), The Ocean Response to Volcanic Iron Fertilisation after the Eruption of Kasatochi Volcano: A Regional-Scale Biogeochemical Ocean Model Study, *Biogeosciences*, *10*(6), 3715-3729.

MacIntyre, H.L., Kana, T.M., Anning, T., and R.J. Geider (2002) Photoacclimation of photosynthesis irradiance response curves and photosynthetic pigments in microalgae and cyanobacteria. J. Phycol. 38: 17-38.

Marchetti, A., & Harrison, P. J. (2007), Coupled Changes in the Cell Morphology and the Elemental (C, N, and Si) Composition of the Pennate Diatom Pseudo-Nitzschia Due to Iron Deficiency, *Limnology and Oceanography*, *52*(5), 2270-2284.

Martin, J. H., & Fitzwater, S. E. (1988), Iron-Deficiency Limits Phytoplankton Growth in the Northeast Pacific Subarctic, *Nature*, *331*(6154), 341-343.

Martin, J. H., Gordon, R. M., & Fitzwater, S. E. (1991), The Case for Iron, *Limnology and Oceanography*, *36*(8), 1793-1802.

McAllister, C. D. (1969), Aspects of Estimating Zooplankton Production from Phytoplankton Production, *Journal of the Fisheries Research Board of Canada*, *26*(2), 199-+.

Melancon, J., Levasseur, M., Lizotte, M., Delmelle, P., Cullen, J., Hamme, R. C., et al. (2014), Early Response of the Northeast Subarctic Pacific Plankton Assemblage to Volcanic Ash Fertilization, *Limnology and Oceanography*, *59*(1), 55-67.

Olgun, N., Duggen, S., Croot, P. L., Delmelle, P., Dietze, H., Schacht, U., et al. (2011), Surface Ocean Iron Fertilization: The Role of Airborne Volcanic Ash from Subduction Zone and Hot Spot Volcanoes and Related Iron Fluxes into the Pacific Ocean, *Global Biogeochemical Cycles*, *25*.

Pavolonis, M. J., Heidinger, A. K., & Sieglaff, J. (2013), Automated Retrievals of Volcanic Ash and Dust Cloud Properties from Upwelling Infrared Measurements, *Journal of Geophysical Research-Atmospheres*, *118*(3), 1436-1458.

Pavolonis, M. J., Feltz, W. F., Heidinger, A. K., & Gallina, G. M. (2006), A Daytime Complement to the Reverse Absorption Technique for Improved Automated Detection of Volcanic Ash, *Journal of Atmospheric and Oceanic Technology*, *23*(11), 1422-1444.

Prata, A. J. (1989), Observations of Volcanic Ash Clouds in the 10-12-Mu-M Window Using Avhrr/2 Data, *International Journal of Remote Sensing*, *10*(4-5), 751-761.

Price, N. M., Andersen, L. F., & Morel, F. M. M. (1991), Iron and Nitrogen Nutrition of Equatorial Pacific Plankton, *Deep-Sea Research Part a-Oceanographic Research Papers*, *38*(11), 1361-1378.

Randles, C. A., da Silva, A. M., Buchard, V., Colarco, P. R., Darmenov, A., Govindaraju, R., et al. (2017), The Merra-2 Aerosol Reanalysis, 1980 Onward. Part I: System Description and Data Assimilation Evaluation, *Journal of Climate*, *30*(17), 6823-6850.

Schrader, P. S., Milligan, A. J., & Behrenfeld, M. J. (2011), Surplus Photosynthetic Antennae Complexes Underlie Diagnostics of Iron Limitation in a Cyanobacterium, *Plos One*, *6*(4).

Siegel, D. A., Behrenfeld, M., Maritorena, S., McClain, C. R., Antoine, D., Bailey, S. W., et al. (2013a), Regional to Global Assessments of Phytoplankton Dynamics from the Seawifs Mission, *Remote Sensing of Environment*, *135*, 77-91.

Siegel, D. A., Behrenfeld, M. J., Maritorena, S., McClain, C. R., Antoine, D., Bailey, S. W., et al. (2013b), Regional to Global Assessments of Phytoplankton Dynamics from the Seawifs Mission, *Remote Sensing of Environment*, *135*(0), 77-91.

Six, C., Finkel, Z.V., Rodriguez, F., Marie, D., Partensky, F., and D.A. Campbell (2008), Contrasting photoacclimation costs in ecotypes of the marine eukaryotic picoplankter Ostreococcus. Limnology and oceanography 53(1), 255–265.

Strzepek, R. F., & Harrison, P. J. (2004), Photosynthetic Architecture Differs in Coastal and Oceanic Diatoms, *Nature*, *431*(7009), 689-692.

Strzepek, R.F., Boyd, P.W., Sunda, W.G. (2019), Photosynthetic adaptation to low iron, light, and temperature in Southern Ocean phytoplankton, Proceedings of the National Academy of Sciences, 16 (10), 4388-4393.

Sunda, W. G., & Huntsman, S. A. (1995), Iron Uptake and Growth Limitation in Oceanic and Coastal Phytoplankton, *Marine Chemistry*, *50*(1-4), 189-206.

Sunda, W. G., & Huntsman, S. A. (1997), Interrelated Influence of Iron, Light and Cell Size on Marine Phytoplankton Growth, *Nature*, *390*, 389-392.

Tsuda, A., Takeda, S., Saito, H., Nishioka, J., Nojiri, Y., Kudo, I., et al. (2003), A Mesoscale Iron Enrichment in the Western Subarctic Pacific Induces a Large Centric Diatom Bloom, *Science*, *300*(5621), 958-961.

Waite, A.M., Nodder, S.D. (2001) The e!ect of in situ iron addition on the sinking rates and export #ux of Southern Ocean diatoms. Deep-Sea Research II 48, 2635-2654.

Waythomas, C. F., Scott, W. E., Prejean, S. G., Schneider, D. J., Izbekov, P., & Nye, C. J. (2010), The 7-8 August 2008 Eruption of Kasatochi Volcano, Central Aleutian Islands, Alaska, *Journal of Geophysical Research-Solid Earth*, *115*.

Werdell, P. J., Franz, B. A., Bailey, S. W., Feldman, G. C., Boss, E., Brando, V. E., et al. (2013), Generalized Ocean Color Inversion Model for Retrieving Marine Inherent Optical Properties, *Applied Optics*, *52*(10), 2019-2037.

Westberry, T., Behrenfeld, M. J., Siegel, D. A., & Boss, E. (2008), Carbon-Based Primary Productivity Modeling with Vertically Resolved Photoacclimation, *Global Biogeochemical Cycles*, *22*(2).

Westberry, T. K., Behrenfeld, M. J., Milligan, A. J., & Doney, S. C. (2013), Retrospective Satellite Ocean Color Analysis of Purposeful and Natural Ocean Iron Fertilization, *Deep-Sea Research Part I-Oceanographic Research Papers*, *73*, 1-16.

Westberry, T. K., Schultz, P., Behrenfeld, M. J., Dunne, J. P., Hiscock, M. R., Maritorena, S., et al. (2016), Annual Cycles of Phytoplankton Biomass in the Subarctic Atlantic and Pacific Ocean, *Global Biogeochemical Cycles*, *30*(2), 175-190.

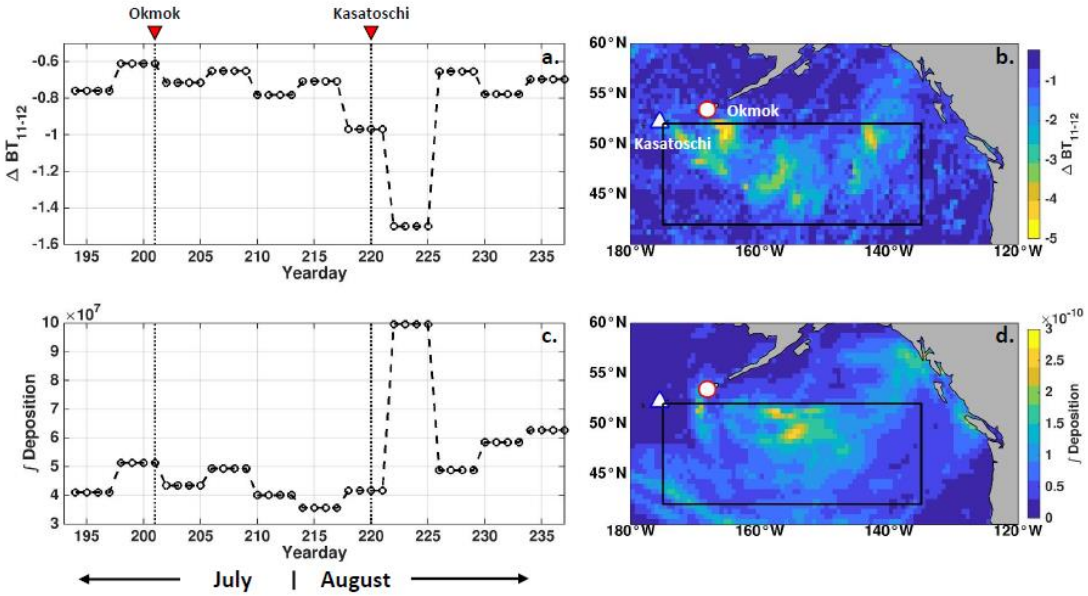

Figure 1. Volcanic ash plumes and deposition as characterized by atmospheric remote sensing and model products in the Subarctic Pacific during summer 2008. **a)** 4-day composite time series of MODIS-derived brightness temperature difference between 11 and 12 μm ($\Delta BT_{11\text{-}12}$). Solid line shows time series linearly interpolated between first day of each 4-day period, dashed line assumes same value for each day of 4-day period. Dotted vertical lines indicate initiation of eruption for Okmok (YD 201) and Kasatoschi (YD 220). **b)** MODIS $\Delta BT_{11\text{-}12}$ for the 4-day period following Kasatoschi eruption (YD 222-225), **c)** MERRA2 area-integrated aerosol deposition (kg d^{-1}) over the analysis region. **d)** MERRA2 daily aerosol deposition (kg m^{-2} s^{-1}) for the 4-day period following Kasatoschi eruption (YD 222-225). Time series in a) and c) are averaged over the analysis region bounded by black box (44-54°N, 135-175°W). Location of Okmok and Kasatoschi shown by filled circle and triangle, respectively.

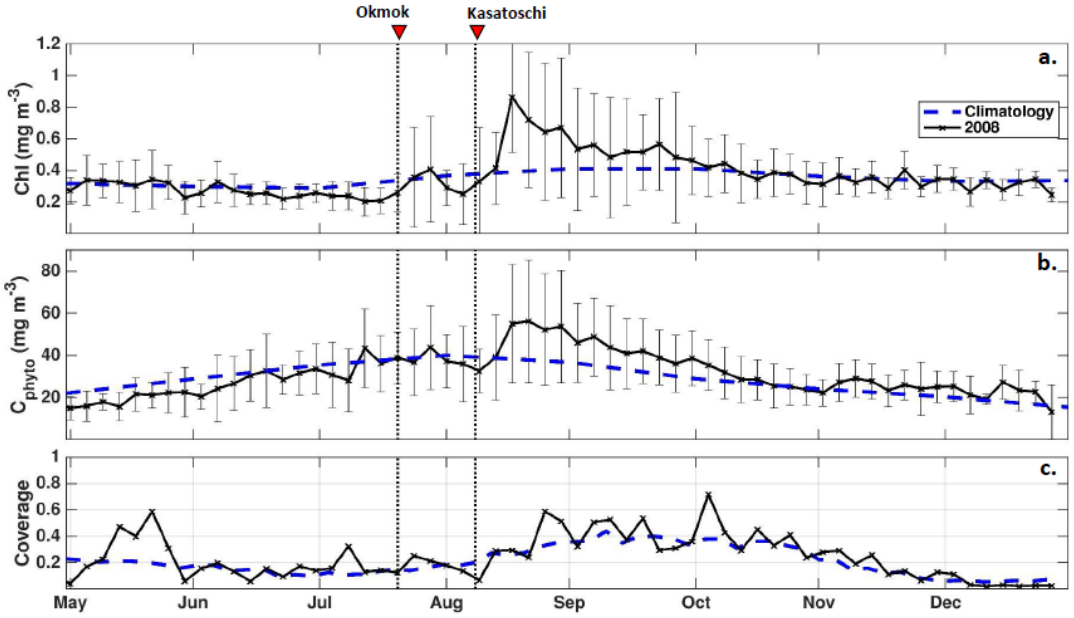

Figure 2. Bulk ocean color properties in Subarctic Pacific during 2008 from satellite remote sensing. **a)** 4-day composite times series of chlorophyll concentration for 2008 (black line), errorbars represent spatial variability within analysis region at each 4-day interval and are calculated as the mean difference between the 16th and 84th percentile of the data (equivalent to standard deviation for normally distrusted data). Monthly mission-era climatology (2003-2017) also shown (blue dashed line). Dotted vertical lines indicate initiation of eruption for Okmok (YD 201) and Kasatoschi (YD 220). **b)** Similar to panel a), but for phytoplankton carbon biomass (C_{phyto}). **c)** Fractional coverage of valid ocean color retrievals within analysis region at each 4-day interval. Analysis region bounded by black box in Figure 1b (44-54°N, 135-175°W).

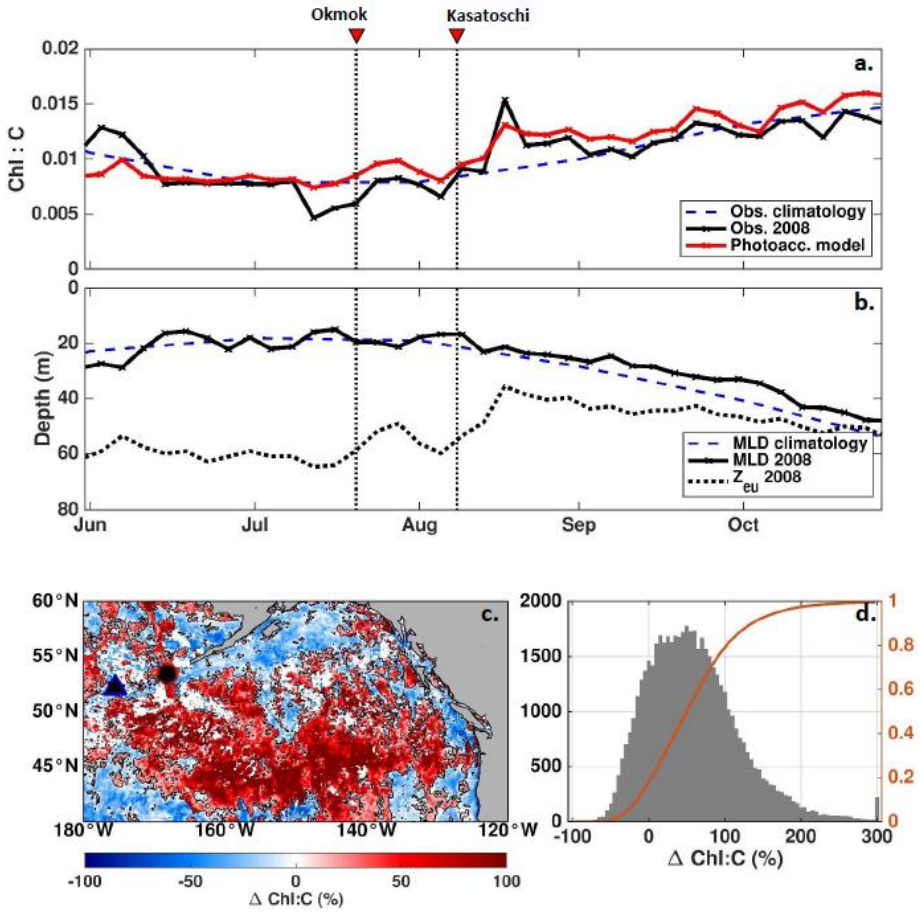

Figure 3. Phytoplankton physiological response following volcanic eruptions in summer 2008. **a)** 4-day composite times series of Chl:C during 2008 (black line), photoacclimation model-predicted Chl:C (red line), and monthly mission-era climatology (blue dashed line). Dotted vertical lines indicate initiation of eruption for Okmok (YD 201) and Kasatoschi (YD 220). **b)** 4-day composite time-series of mixed layer depth (MLD, solid black line) and euphotic depth (Zeu, dotted black line). Monthly climatological MLD also shown (dashed blue line). **c)** Monthly relative anomaly in Chl:C for August 2008, ΔChl:C (%). **d)** Histogram of ΔChl:C within bounding box shown in Figure 1. Also shown is the cumulative distribution function (orange line and right-hand y-axis).

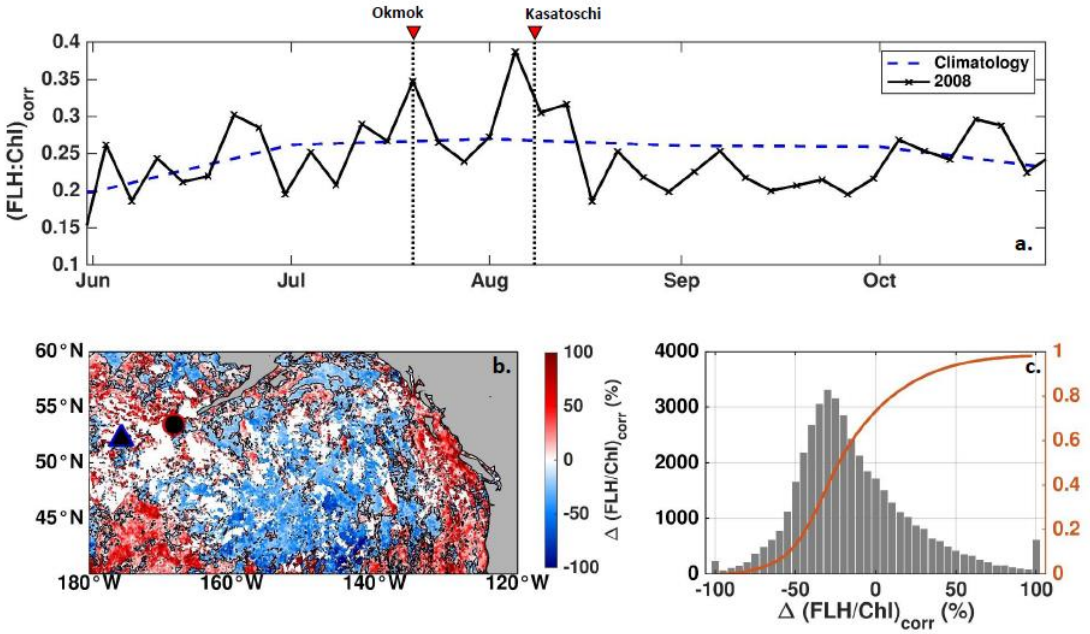

Figure 4. Satellite chlorophyll fluorescence following volcanic eruptions in summer 2008. a) 4-day composite time series of fluorescence yield corrected for light-induced non-photochemical quenching $(nFLH:Chl)_{corr}$, black line). Monthly mission-era climatology also shown (blue dashed line). Dotted vertical lines indicate initiation of eruption for Okmok (YD 201) and Kasatoschi (YD 220). **b)** Monthly anomaly in NPQ-corrected fluorescence yield for August 2008, $\Delta(nFLH:Chl)_{corr}$. **c)** Histogram of $\Delta(nFLH:Chl)_{corr}$ within bounding box shown in Figure 1. Also shown is the cumulative distribution function (orange line and right-hand y-axis).